

Nonparametric estimation of the size and waiting time distributions of pulsar glitches

G. Howitt¹, A. Melatos¹, and A. Delaigle²,

ghowitt@student.unimelb.edu.au, amelatos@unimelb.edu.au

ABSTRACT

Glitch size and waiting time probability density functions (PDFs) are estimated for the five pulsars that have glitched most using the nonparametric kernel density estimator. Two objects exhibit decreasing size and waiting time PDFs. Their activity is Poisson-like, and their size statistics are approximately scale-invariant. Three objects exhibit a statistically significant local maximum in the PDFs, including one (PSR J1341–6220) which was classified as Poisson-like in previous analyses. Their activity is quasiperiodic, although the dispersion in waiting times is relatively broad. The classification is robust: it is preserved across a wide range of bandwidth choices. There is no compelling evidence for multimodality, but this issue should be revisited when more data become available. The implications for superfluid vortex avalanche models of pulsar glitches are explored briefly.

Subject headings: dense matter — pulsars: general — stars: interior — stars: neutron — stars: rotation

1. Introduction

Rotational glitches are impulsive, irregularly spaced spin-up events observed in pulsars. The discovery of glitches came soon after the birth of pulsar astronomy itself: the first glitch was detected in the Vela pulsar in 1968 (Radhakrishnan & Manchester 1969; Reichley & Downs 1969), and in 1969 the first glitch was discovered in the Crab pulsar (Nelson et al. 1970; Lyne et al. 1993). Glitches have been discovered through large-scale monitoring programs with multibeam receivers at the Parkes and Jodrell Bank Observatories (Espinoza et al. 2011; Yu et al. 2013). At the time of writing, 504 (430) events have been detected

¹School of Physics, University of Melbourne, Parkville, VIC 3010, Australia

²Department of Mathematics and Statistics, University of Melbourne, Parkville, VIC 3010, Australia

in 187 (143) objects¹, amounting to $\sim 10\%$ of the known pulsar population. The glitch catalogues record the instantaneous fractional change in the pulse frequency at the time of the glitch, known as the glitch size, $\Delta\Omega/\Omega$, and the epoch when each glitch occurs. From the epochs, we calculate the waiting time, Δt , as the difference between the epochs of successive glitches.

Glitches are thought to be caused by sudden readjustments within neutron stars; see Haskell & Melatos (2015) for a recent review of theoretical glitch models. Studying the statistical properties of glitches may therefore lead to new insights into the physics of dense nuclear matter. Previous statistical studies can be split into two categories: those that examine the population of glitching pulsars in aggregate, and those that examine the properties of individual pulsars. In the first category, we mention the work of Morley & García-Pelayo (1993), who used size data to fit a power law to the energy released during glitches, and Lyne et al. (2000), who looked at a sample of 32 glitches in 15 pulsars reported in Shemar & Lyne (1996) and found a correlation between glitch activity and spin-down rate. More recently, Fuentes et al. (2017) studied a sample of 384 glitches in 141 pulsars and found a correlation between glitch activity and the spin-down luminosity of the pulsar. Fuentes et al. (2017) also examined glitch sizes in aggregate and found evidence for a multimodal size probability density function (PDF) by fitting a mixed Gaussian model to the histogram of the data. A similar analysis (with similar results) was performed by Konar & Arjunwadkar (2014). In the second category, we mention the work of Melatos et al. (2008), who constructed the empirical cumulative density functions (CDFs) of glitch sizes and waiting times for the nine pulsars with the most recorded glitches and tested for consistency with avalanche models of glitch activity (Warszawski & Melatos 2011; Warszawski et al. 2012; Warszawski & Melatos 2013). Melatos et al. (2008) found that two pulsars, PSR J0537–6910 and PSR J0835–4510, differ from the rest of the pulsars studied in both their size and waiting time PDFs, a finding also reported in Espinoza et al. (2011). Onuchukwu & Chukwude (2016) performed a similar analysis on ‘microglitches’ (jumps in pulsar frequency with $|\Delta\Omega/\Omega| \sim 10^{-10}$) in 20 pulsars using data from the Hartebeesthoek radio telescope and again interpreted the results in the context of avalanche processes. Studies of the most active glitching pulsar, PSR J0537–6910, reveal a strong linear correlation between size and waiting time to the following glitch (Middleitch et al. 2006; Ferdman et al. 2017; Antonopoulou et al. 2018). Similarly, Shaw et al. (2018) claimed to find a correlation in PSRJ 0534+2200 between size and waiting time since

¹ Up-to-date catalogues are kept by the Jodrell Bank Centre for Astrophysics at <http://www.jb.man.ac.uk/pulsar/glitches.html> and the Australia Telescope National Facility (ATNF) at <http://www.atnf.csiro.au/research/pulsar/psrcat/glitchTbl.html>. Numbers quoted in the text without (with) parentheses refer to the Jodrell Bank (ATNF) data. Numbers are current as at 2018 May 28.

the previous glitch. Eya et al. (2017) found that the size PDF in 12 pulsars is well fitted by a normal distribution.

Statistical glitch studies usually posit functional forms for the size and waiting time distributions, e.g. finite mixture models (Konar & Arjunwadkar 2014), or normal distributions (Eya et al. 2017). These methods assume that a set of global parameters define the PDF across its domain. By contrast, a nonparametric estimator makes no assumptions about the global form of the PDF but instead estimates the local probability density around each data point (Hall 1992)². Nonparametric estimators are widely used in a host of scientific applications (Silverman 1986). Recently, nonparametric estimation has been used as an independent way to verify the discovery of two interesting new features in the Crab pulsar: a resolved minimum glitch size (Espinoza et al. 2014), and an 11-year episode of accelerated glitch activity (Lyne et al. 2015). In another recent application of nonparametric estimation in pulsar glitch research, Ashton et al. (2017) estimated the size distribution of all glitches to assess whether glitches will impact the discovery of gravitational waves from rotating neutron stars. In this paper, we study the individual glitch size and waiting time PDFs for the five pulsars with the highest number of recorded glitches using the kernel density estimator (Wand & Jones 1995).

We review the algorithm briefly, and evaluate its performance, in §2. We then apply the algorithm to construct waiting time and size PDF estimates for the most active glitchers in §3.1 and §3.2 respectively, and the case for multimodality in certain objects is examined critically. We compare the results with previous parametric studies and astrophysical models in §4. The results strengthen the empirical basis for theoretical work, e.g. by firming up the identification of distinct classes of glitching pulsars. They also offer a guide to designing the next generation of glitch monitoring campaigns with phased radio arrays like LOFAR (Kramer & Stappers 2010), UTMOST (Caleb et al. 2016) and the Square Kilometer Array.

2. Kernel density estimator

2.1. Definition

We begin by defining the nonparametric kernel density estimator (Wand & Jones 1995) we use to estimate the PDFs of glitch sizes and waiting times. Let x_1, \dots, x_N be N independent, identically distributed samples of a random variable x , with underlying PDF

² The astrophysicist reader may recognize this as the fundamental idea behind smoothed particle hydrodynamics (Monaghan 2005).

$p(x)$. The kernel density estimator $\hat{p}(x)$ of $p(x)$ is given by

$$\hat{p}(x) = \frac{1}{N} \sum_{i=1}^N K\left(\frac{x - x_i}{h}\right), \quad (1)$$

where $K(x)$ is a symmetric, positive definite kernel function $K(x)$ with normalization $\int dy K(y) = 1$. The output of the kernel density estimator is usually insensitive to the exact shape of $K(x)$. Truncated polynomials and smooth functions multiplied by a Gaussian are common choices (Wand & Jones 1995), and these kernels produce an equivalent kernel density estimate under an appropriate rescaling of the bandwidth (Marron & Nolan 1988). An exception is sharply peaked distributions, such as atomic spectra, where a different class of kernels known as ‘infinite order kernels’ are more appropriate (Davis 1975, 1977). In this paper, we use a Gaussian kernel exclusively; the kernel corresponding to the datum x_i is

$$K_i(x) = \frac{1}{h\sqrt{2\pi}} \exp\left[-\frac{1}{2}\left(\frac{x - x_i}{h}\right)^2\right]. \quad (2)$$

The value of the estimator at x is a weighted tally of the observations x_i in a neighborhood $|x - x_i| \lesssim h$ of x ; or, equivalently, it is the unweighted sum of N identical copies of the kernel function, centered at x_1, \dots, x_N . Either way, each data point is spread across several bins to give a smoothly differentiable PDF. Kernel density estimation has achieved broad acceptance in many applications because it represent a more optimal trade-off between bias and variance than a bin-centred histogram. We also note that a bin-centred histogram is a kernel density estimator with a rectangular function as the kernel; in this work we use a Gaussian kernel so that the estimator inherits the useful properties of continuity and differentiability.

The key challenge when applying Equation (1) is to select the bandwidth h in a way that ensures good practical performance. The ensemble-averaged, x -integrated bias $\int dx \langle \hat{p}(x) - p(x) \rangle$ and variance $\int dx \langle [\hat{p}(x) - p(x)]^2 \rangle$ increase and decrease respectively, as h increases in the limit $N \rightarrow \infty$. Hence optimizing h involves a compromise between bias and variance. One approach is to let h vary with x according to the local density of data points (see footnote 2) but it is ill-suited to small glitch samples. An alternative, which has proven its worth in many applications, is to choose a single, global h , that minimizes the asymptotic mean integrated square error (Wand & Jones 1995),

$$\text{AMISE} = \frac{1}{Nh} \int dx [K(x)]^2 + \frac{h^4}{4} \left[\int dx x^2 K(x) \right]^2 \int dx [p''(x)]^2. \quad (3)$$

As $p''(x)$ is unknown a priori, it must be approximated. Many techniques have been developed to estimate $p''(x)$ in order to select h to minimise the AMISE [a summary of several of

the more common techniques can found in Wand & Jones (1995)]; in this work we use the normal reference bandwidth³, which assumes that $p(x)$ is a Gaussian with variance σ^2 . In this case, the h that minimises the AMISE can be written analytically,

$$h = \left\{ \frac{8\pi^{1/2} \int dx [K(x)^2]}{3N[\int dx x^2 K(x)^2]} \right\}^{1/5} \sigma. \quad (4)$$

The normal reference bandwidth rule replaces the true variance in equation (4) with some estimate $\hat{\sigma}^2$ (Silverman 1986; Scott 1992). We take $\hat{\sigma}$ to be the minimum of the sample’s interquartile range and standard deviation. It is important to realise that the AMISE is, as the name implies, an asymptotic measure. An h chosen to minimise the AMISE is just an approximation to the bandwidth that truly optimizes the trade-off between bias and variance in the $N \leq 35$ regime of pulsar glitch statistics. In §2.4 we explore the effect of bandwidth selection on synthetic data drawn from a bimodal distribution. In §3 we examine how the estimated PDFs change qualitatively with h .

2.2. Positive definite variables

If a PDF is defined on a finite domain and is non-zero at an endpoint, the kernel density estimator overflows the boundary. Relative to an estimator that takes the boundary into account, the local bias $\langle \hat{p}(x) - p(x) \rangle$ in the vicinity of the boundary is greater than the x -integrated bias $\int dx \langle \hat{p}(x) - p(x) \rangle$. When Equation (1) is applied to a positive definite random variable, such as glitch size or waiting time, probability leaks spuriously into the region $x < 0$. Leakage is significant, when a sizable fraction of the data points satisfy $x_i \lesssim h$. Renormalization does not fix the problem, as it introduces extra bias near $x = 0$. Many methods have been developed to counteract leakage. Here we describe two procedures which are robust and straightforward to implement: (i) reflect the data about $x = 0$ and apply (1) with a symmetric kernel;⁴ or (ii) transform the data (e.g. by taking their logarithm). Taking the logarithm compresses the domain of the size variable (which can otherwise extend over 4 dex in an individual object), so that it can be modelled usefully by a single, global h chosen

³This is, in effect, a second-order parametric assumption. The normal reference bandwidth tends to produce an ‘oversmoothed’ estimate, sacrificing bias in order to reduce variance, and is more appropriate in the small- N regime than other techniques such as Sheather-Jones plug-in (Sheather & Jones 1991) and smoothed cross-validation (Hall et al. 1992).

⁴ One can also reflect about a right-hand boundary, but this is irrelevant for glitches, whose observed sizes and waiting times are much smaller than the maxima that radio timing experiments can detect.

according to (2). We apply the reflection method to the waiting time data in §3.1 and the logarithmic transform method to the size data in §3.2.

2.3. Error estimation with nonparametric methods

An obvious question when using the kernel density estimator is how accurate are the estimates produced? When using a parametric estimator, one can construct confidence intervals by varying the parameters within a range and testing the likelihood of excluding the resulting fit, e.g. with a K-S test as in Figures 2 and 3. With the kernel density estimator, a similar approach is hindered by two issues: the set of estimated parameters is large (formally the number of points where the curve is estimated), and bias is one of the main contributors to the inaccuracy of the estimate (cf. parametric estimators, where the variance dominates) (Hall 1992; Chaudhuri & Marron 1999). One approach to constructing confidence intervals that may seem appealing is to create data replicates by resampling and construct \hat{p} for the replicated data sets. The simplest resampling ‘bootstrapping’ method is inappropriate, because it produces a zero-bias confidence interval on the estimate \hat{p} rather than on the true PDF (Hall 1992). Rather than seeking to construct a (potentially misleading) quantitative measure of the goodness of fit, we instead take a qualitative approach, which aims to test whether particular features of the estimated distribution, e.g. monotonicity and multimodality, are robust features that appear for a wide range of bandwidth choices (Chaudhuri & Marron 1999; Marron & Chung 2001). This concept is discussed further in §2.4 and §3 below.

2.4. Validation

Before analyzing actual data, we run some tests on synthetic data drawn from the exponential distribution $p(x) = e^{-x}$, which acts as a proxy for the glitch waiting time distribution, and the power law distribution $p(x) = 0.2x^{-1.2}$, $x \geq 1$ (Melatos et al. 2008) The tests are not a substitute for definitive convergence studies presented elsewhere (Silverman 1986) but give some sense of the reliability of the estimator and, importantly, the sorts of artifacts (e.g. wiggles, plateaus) that arise from noise. To construct kernel density estimates, we use the statistical software R (R Core Team 2014), and the `bkde` function included in the package `KernSmooth` (Wand 2014).

Figure 1 illustrates qualitatively how the estimator (1) performs with N , when the underlying PDF is an exponential (top row) or a power law (bottom row). For the exponential

distribution, the reflection boundary correction described in §2.2 is used. For the power law distribution, the kernel density estimate is applied to the logarithm⁵ of x . Applying the estimate to $\log_{10}(x)$ reduces fluctuations (bumps and large gaps) that would otherwise appear, so that a global bandwidth gives good performance. As the domain is restricted to $x \geq 1$, and the probability density is significant at $x = 1$, we apply the reflection method to the logarithmic data at $\log_{10} x = 0$. In the top left panel, the colored curves show $\hat{p}(x)$ for three individual realizations with $N = 25, 100$, or 1000 for the exponential distribution (solid black curve). The bottom left panel shows $\hat{p}[\log_{10}(x)]$ for three realizations with $N = 25, 100$, or 1000 , for the power law distribution (solid black line). In the right column, each solid gold curve shows $\hat{p}(x)$ and $\hat{p}[\log_{10}(x)]$ for one realisation with $N = 25$, in order to give a sense of the scatter in the estimator. We have checked many realizations and the results consistently exhibit the following properties. (i) Wiggles appear in $\hat{p}(x)$ for $N \leq 100$. They are noise artifacts, which should not be interpreted as multimodality when analysing real data in §3. (ii) Broadly speaking, the estimator performs similarly on the power law and the exponential. (iii) The estimator plateaus at $x = 0$, when the data are reflected (top row), because K being symmetric implies $\hat{p}'(0) = 0$. Hence $\hat{p}(x)$ systematically underestimates $p(x)$ near $x = 0$, if the underlying PDF is cuspy there, although the bias decreases in a controlled fashion as N increases⁶. In the top-right panel, $\langle \hat{p}(x = 0)/p(x = 0) \rangle = 0.71$, with a standard deviation of 0.18; in the bottom-right panel, $\langle \hat{p}[\log_{10}(x)]/p[\log_{10}(x)] \rangle = 0.72$, with a standard deviation of 0.2.

Another issue worth addressing is the performance of the kernel density estimator for multimodal PDFs, which have been proposed for glitch sizes in previous aggregated studies (Konar & Arjunwadkar 2014; Ashton et al. 2017; Fuentes et al. 2017) and in analyses of individual pulsars (Melatos et al. 2008). We aim to determine whether the kernel density estimator can reliably reproduce multiple peaks in a PDF as h varies. As a test, we consider a bimodal PDF obtained by summing two Gaussians, viz. $p(x) = 0.6\mathcal{N}(\mu = 4, \sigma = 1) + 0.4\mathcal{N}(\mu = 8, \sigma = 1)$, where $\mathcal{N}(\mu, \sigma)$ is the normal distribution with mean μ and standard deviation σ . We draw a variate of dimension $N = 25$ from $p(x)$, and construct the kernel density estimate with three choices of bandwidth: the normal reference bandwidth, h_0 , as well as $h_0/2$, and $2h_0$. The results are shown in Figure 2

Figure 2 illustrates the characteristic property (Silverman 1986) of the kernel density

⁵If a variable x is distributed according to a power law, i.e. $p(x) \propto x^{-a}$, then the PDF of the logarithmic variable $y = \log_{10}(x)$ obeys $q(y) \propto (10^y)^{1-a}$.

⁶ In the absence of reflection, leakage can underestimate $p(x = 0)$ by up to a factor of two, independent of N . One can recognise this by noting that the positive and negative points in the reflected data contribute equally to $\hat{p}(x = 0)$.

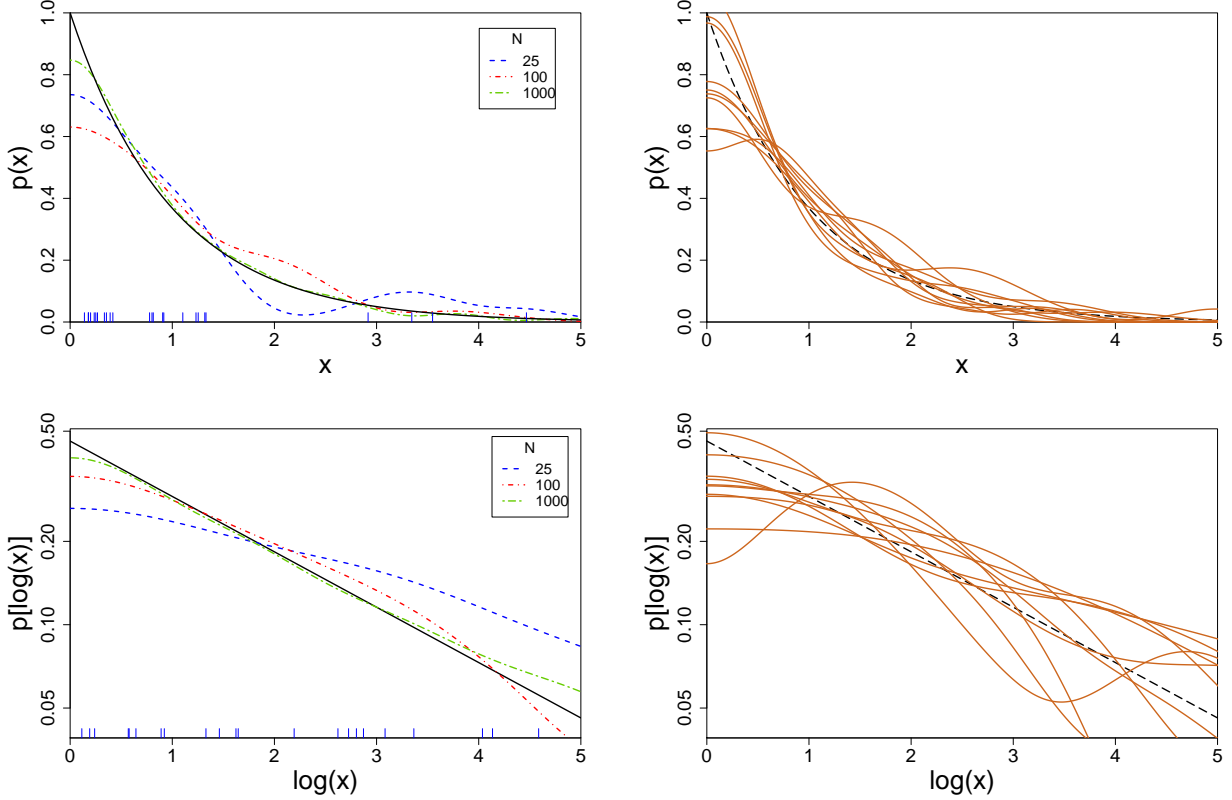


Fig. 1.— Convergence of the kernel density estimator $\hat{p}(x)$ [equation (1)] for an exponential PDF, $p(x) = e^{-x}$ (top row), and $\hat{p}[\log_{10}(x)]$ for the power law PDF, $p(x) = 0.2x^{-1.2}$ with $x \geq 1$ (bottom row). The solid black curve in the top row corresponds to the exponential PDF, The solid, colored curves in the left column correspond to $\hat{p}(x)$ and $\hat{p}[\log_{10}(x)]$ for realizations with $N = 25$ (blue), 100 (red), and 1000 (green). The tick marks in the panels in the left column indicate the abscissae of the data in the $N = 25$ (blue) realizations. The dashed black line in the bottom row shows the power law PDF. The right-hand column shows 10 instances of $\hat{p}(x)$ and $\hat{p}[\log_{10}(x)]$ with $N = 25$ (gold curves). Equation (1) is applied to the reflected data in the top row and the reflected base-10 logarithm of the data in the bottom row.

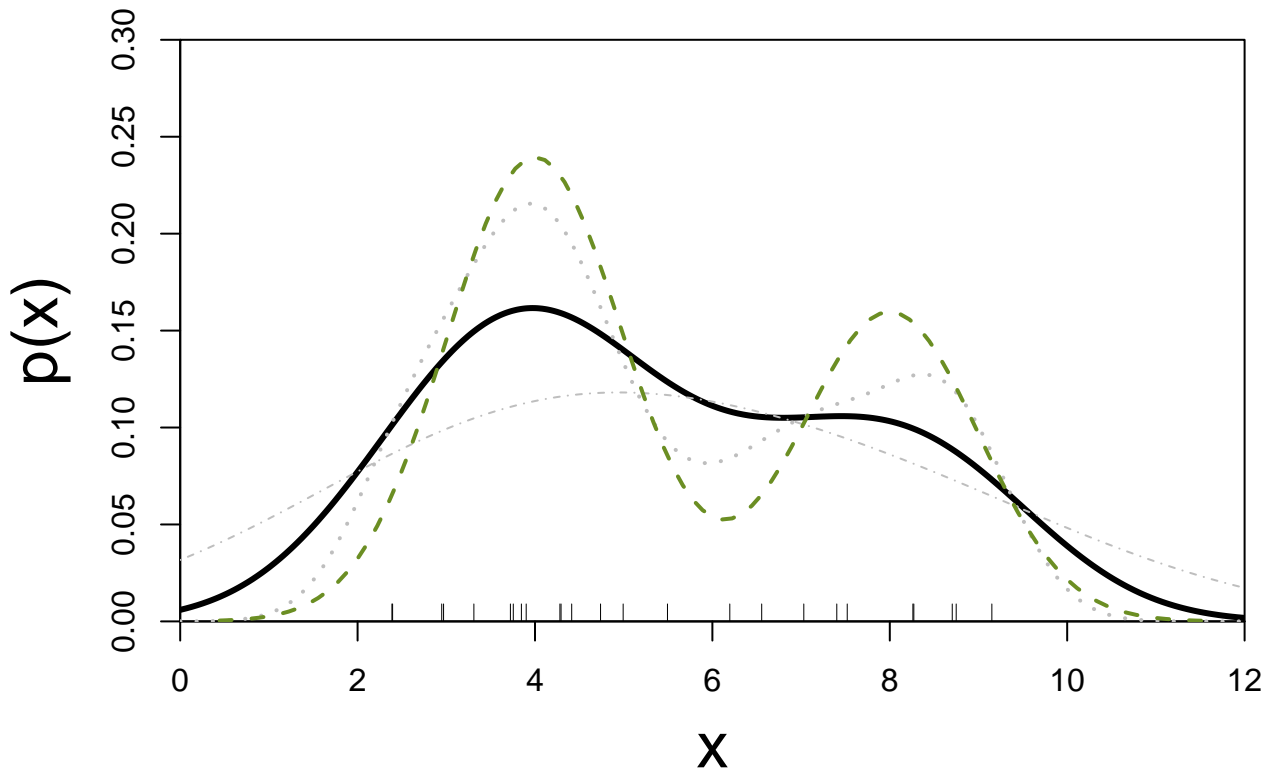


Fig. 2.— Kernel density estimates of a two-component Gaussian PDF $p(x) = 0.6\mathcal{N}(\mu = 4, \sigma = 1) + 0.4\mathcal{N}(\mu = 8, \sigma = 1)$, with $N = 25$ data points. The solid black curve shows the kernel density estimate with bandwidth h_0 chosen by the normal reference rule, the dotted grey curve is the kernel density estimate with bandwidth $h_0/2$ and the dot-dashed grey curve is with bandwidth $2h_0$. The dashed green curve shows the underlying PDF from which the data used to construct the estimator, shown as black tick marks along the x -axis, are drawn.

estimator with the normal reference bandwidth: the features of the underlying PDF are recovered in the estimator, which has local maxima at $x \approx 4$ and $x \approx 8$, but the estimator is somewhat ‘oversmoothed’, with $p(x)$ at the peaks underestimated by $\approx 30\%$ and $p(x)$ at the minimum overestimated by a factor of ≈ 2 . The estimator with $h = h_0/2$ tends closer to the underlying PDF, however, the location of the peaks is less accurate. The estimator with $h = 2h_0$ is excessively oversmoothed, as it completely fails to capture the bimodality in $p(x)$, instead producing a single, broad peak centered about $x \approx 5$. As Figure 1 shows, it is possible for the kernel density estimator to produce local maxima even when the underlying PDF is monotonic, so we tend to prefer the normal reference bandwidth with its tendency to slightly oversmooth. However, in our analysis of glitch data in §3 we use the same set of bandwidths as in Figure 2 in order to illustrate the uncertainty inherent to the method (Chaudhuri & Marron 1999).

3. Probability density functions

According to the Jodrell Bank catalogue at 2018 May 28, 504 glitches have been detected in 187 pulsars⁷. Yu & Liu (2017) performed a detectability study of glitches in the Yu et al. (2013) data set and concluded that all detectable glitches in these data had been identified. Espinoza et al. (2014) performed a detectability study of glitches in the Crab pulsar with Jodrell Bank data and reached the same conclusion; see also Janssen & Stappers (2006). Other than these two studies, however, no other authors have presented results on the completeness of glitch catalogues. We stress that both the Jodrell Bank and the ATNF glitch catalogues may not be complete, and our analysis in this paper may be based on an incomplete data set. In addition to the glitches in the Jodrell Bank catalogue, approximately 20 additional glitches have been reported in PSR J0537–6910 in two papers by Ferdman et al. (2017); Antonopoulou et al. (2018). In this section, we construct size and waiting time PDFs for the five objects that have glitched most prolifically: PSR J1740–3015 ($N = 35$), PSR J0534+2200 (26), PSR J0537–6910 (42),⁸ PSR J1341–6220 (23), and PSR J0835–4510 (21). Experience across many scientific applications teaches that one needs $N \gtrsim 20$ to get meaningful nonparametric results (Silverman 1986), as verified by Figure 1. The sample sizes for the next most active objects, PSR J0631+1036 ($N = 15$) and PSR J1801–2304 ($N = 13$), are too small to be analysed nonparametrically [cf. Melatos et al. (2008)]; their

⁷ We work with the larger Jodrell Bank catalogue henceforth and cross-check against the ATNF catalogue.

⁸There is tension in the number of glitches and the parameters of glitches for PSR J0537–6910 between Ferdman et al. (2017); Antonopoulou et al. (2018) and earlier work by Middleditch et al. (2006). We cross-check all three references and include the glitches common to two out of three sources in our analysis.

estimated PDFs are too bumpy.

3.1. Waiting times

Figure 3 displays the waiting time PDFs for the five pulsars selected above. In each panel, the nonparametric kernel density estimator $\hat{p}(\Delta t)$ (units: yr^{-1}) from equation (1), using the normal reference bandwidth, $h = h_0$, is graphed on a linear scale as a solid curve. In the left column of 3, we displays fits to the Poisson PDF, $p(\Delta t) = \lambda e^{-\lambda \Delta t}$. The red dashed curve corresponds to the maximum likelihood estimate $\lambda = \langle \Delta t \rangle^{-1}$. The grey dotted curves correspond to the values of λ which demarcate the interval (λ_-, λ_+) , where the null hypothesis that the data are drawn from a Poisson distribution is rejected by a K-S test with less than 68% confidence (Melatos et al. 2008). In the right-hand column, we display two additional kernel density estimators using different bandwidths. The dashed red curve is with $h = h_0/2$, the dotted blue curve is with $h = 2h_0$.

Figure 3 reveals three important things. First, broadly speaking, $\hat{p}(\Delta t)$ decreases with Δt for PSR J0534+2200 and PSR J1740–3015, notwithstanding the bumps in the body and tail of the PDF estimate and the low- Δt plateau, which are both peculiarities of the kernel density estimator, as implied by Figure 1. It is apparent by eye that $\hat{p}(\Delta t)$ is broadly consistent with the parametric Poisson PDF posited previously (Wong et al. 2001; Melatos et al. 2008; Espinoza et al. 2011); the dashed curve in the left-hand column hugs the solid curve and falls between (and nearly coincides with) the dotted fits from Melatos et al. (2008), even after adding three events since 2008.

Second, $\hat{p}(\Delta t)$ rises to a maximum in the other objects. This is interesting, since PSR J0537–6910 and PSR J0835–4510 are traditionally classified as quasiperiodic glitchers (Middleitch et al. 2006; Melatos et al. 2008), but PSR J1341–6220 was previously classified as Poisson-like (Melatos et al. 2008). The peak in $\hat{p}(\Delta t)$ in the latter object is broad; in fact, the dashed Poisson curve is still a fair fit to the solid curve, albeit displaced downwards. However, $\hat{p}(0)$ is less than 30% of $\hat{p}(\Delta t)$ at the peak for all three non-Poisson-like objects, and the maximum in \hat{p} is at $\Delta t > 0$ using the most oversmoothing bandwidth $h = 2h_0$; suggesting the existence of a maximum at $\Delta t > 0$ instead of $\Delta t = 0$

Third, there is some evidence of bimodality in PSR J0835–4510 and PSR J1341–6220, both of which show local minima in $\hat{p}(\Delta t)$ with $h = h_0$ and $h = h_0/2$. Quasiperiodic glitchers have been modelled with a two-component PDF in previous work (Melatos et al. 2008; Konar & Arjunwadkar 2014; Ashton et al. 2017; Fuentes et al. 2017). In particular, it is sometimes said that the ‘big’ glitches in PSR J0835–4510 are spaced regularly, but the ‘small’ ones are

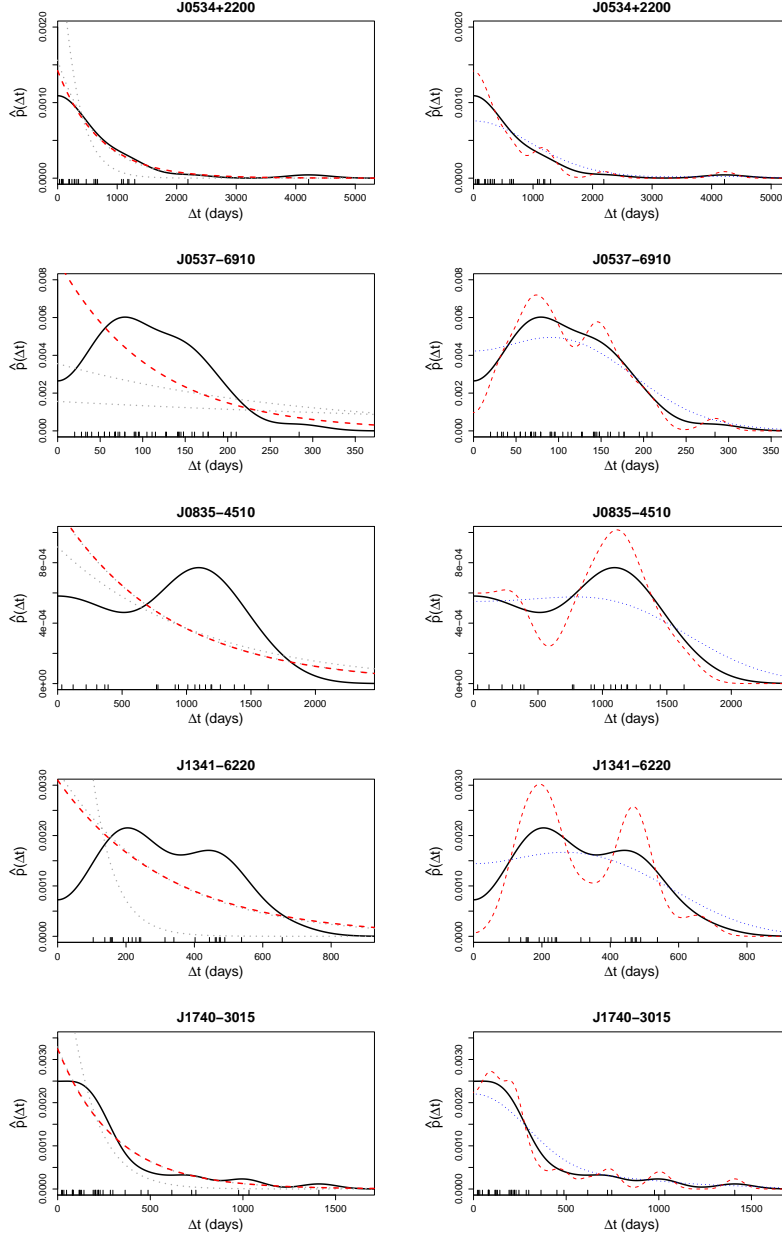


Fig. 3.— Kernel density estimates of the waiting time PDFs $\hat{p}(\Delta t)$ for the five most active glitchers, plotted on linear axes. Solid curves correspond to the nonparametric kernel density estimator with a normal reference bandwidth $h = h_0$. In the left-hand column, red dashed curves are parametric Poisson fits with $\lambda = \langle \Delta t \rangle^{-1}$ (maximum likelihood) computed directly by averaging the data. Grey dotted curves are Poisson fits with $\lambda = \lambda_{\pm}$ from the K-S analysis in Melatos et al. (2008). In the right-hand column, the red dashed curves are the kernel density estimator with bandwidth $h = h_0/2$, the blue dotted curve is with $h = 2h_0$. Tick marks on the horizontal axis indicate the abscissae of the raw data.

not. The short- Δt component, if present, arguably dominates the long- Δt component in PSR J1341–6220, whereas the situation is the other way around in PSR J0835–4510. Looking at $\hat{p}(\Delta t)$ for PSR J0534+2200 and PSR J1740–3015, with $h = h_0/2$, however, shows that this choice of bandwidth significantly ‘undersmooths’ the PDF, producing multiple peaks centred about one or two events. On balance, we do not see convincing evidence for bimodality in $\hat{p}(\Delta t)$ in Figure 3. The gentle bumps in Figure 3 look much like the small- N features identified in the validation experiments in Figure 1 due to sparse sampling of the PDF. More data are required to rule out bimodality definitively, but there are certainly no strong grounds for claiming its existence on the basis of a nonparametric analysis at present.

3.2. Sizes

Figure 4 displays the estimated PDF of the fractional size logarithm, $s = \log_{10}(\Delta\nu/\nu)$. In the left column, the nonparametric estimate $\hat{p}(s)$ from (1) using a normal reference bandwidth, $h = h_0$, is graphed as a solid curve. Also displayed are parametric fits to the power law distribution $p(\Delta\nu) = (1 - a)(\Delta\nu_{\max}^{1-a} - \Delta\nu_{\min}^{1-a})^{-1}\Delta\nu^{-a}$. The exponent a is estimated by maximum likelihood (red dashed line) and by calculating the end-points $a = a_{\pm}$ (grey dotted lines) of $a_- \leq a \leq a_+$, where the K-S probability exceeds 32% as in Figure 2; see Melatos et al. (2008) for details. There is an art to choosing $\Delta\nu_{\min}$ and $\Delta\nu_{\max}$, as discussed in §4.3 in Melatos et al. (2008). The smallest glitch observed is likely to be a reasonable estimate of $\Delta\nu_{\min}$, because $p(\Delta\nu)$ rises steeply as $\Delta\nu \rightarrow 0$, but this has not been quantified systematically except by Janssen & Stappers (2006), who simulated microglitch detection in a noisy time series and found $\Delta\nu_{\min} = 10^{-10}\nu$ for recent Jodrell Bank observations; see also Espinoza et al. (2014), where it is claimed that the lower cut-off in $p(\Delta\nu)$ can be resolved. Below we set $\Delta\nu_{\min}$ and $\Delta\nu_{\max}$ to the observed minimum and maximum respectively; the results are insensitive to this choice, as demonstrated previously (Melatos et al. 2008). If the glitch size distribution truly follows a power law, then it is bounded from below and the estimator $\hat{p}(s)$ should include a reflection boundary correction as in §2.4 and Figure 1. However, we have neglected to perform this boundary correction, since we don’t know where (if anywhere) the boundary is. In the right column of Figure 4, we show $\hat{p}(s)$ with $h = h_0$ as a black solid curve, and also $\hat{p}(s)$ with $h = h_0/2$ (dashed red curve) and $h = 2h_0$ (dotted blue curve).

Figure 4 elaborates the classification stemming from Figure 3 in two interesting ways. First, we find that $\hat{p}(s)$ generally decreases with s , with a prominent peak at $\approx s_{\min}$, for the Poisson-like duo, PSR J0534+2200 and PSR J1740–3015, whose waiting time PDFs also

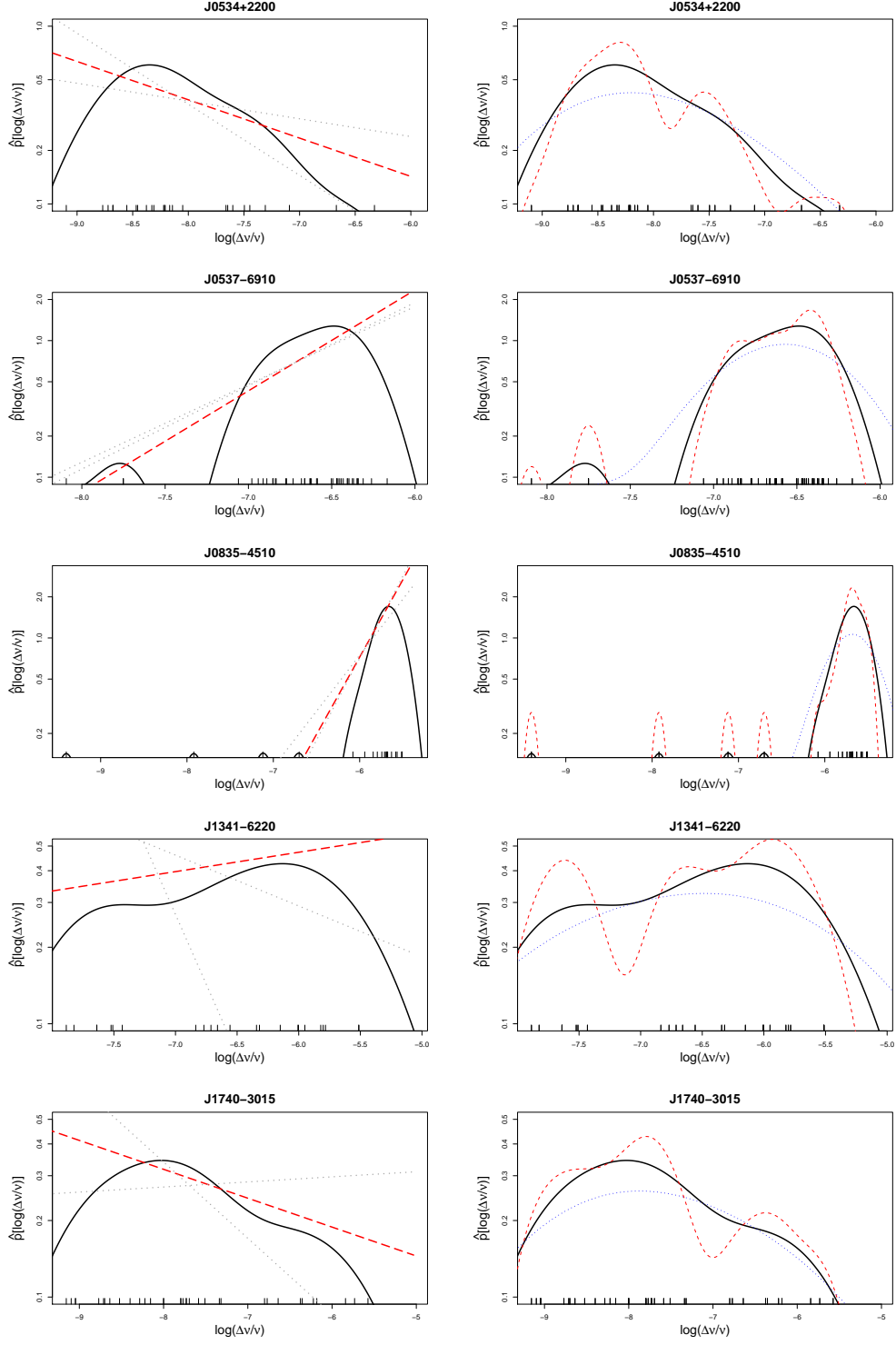


Fig. 4.— Kernel density estimates of the fractional size PDFs $\hat{p}(s)$, for the five most active glitchers, plotted on log-log axes. The solid black curve is $\hat{p}(s)$ using a normal reference bandwidth, $h = h_0$. In the left-hand column, the dashed red lines show the parametric power-law fit with a estimated by maximum likelihood. The grey dotted lines are power-law fits with $a = a_{\pm}$ from the K-S analysis in Melatos et al. (2008). In the right-hand column, the red dashed curves are $\hat{p}(s)$ with $h = h_0/2$, and the blue dotted curves are $\hat{p}(s)$ with $h = 2h_0$. Tick marks on the horizontal axis indicate the abscissae of the raw data.

decrease ⁹. In contrast, PSR J0537–6910 and PSR J0835–4510 are not monotonic, with $\hat{p}(s_{\min})$ less than 20% of $\hat{p}(s)$ at the peak and the bulk of the probability confined within $\lesssim 1$ dex. PSR J1341–6220, previously classified as Poisson-like by Melatos et al. (2008) and now a quasiperiodic candidate on the basis of Figure 1, displays interesting intermediate behavior: $\hat{p}(s)$ does not decrease monotonically but nor is it narrowly peaked, staying nearly flat over ≈ 2 dex. This may mean one of two important things: (i) the broad waiting time plateau in Figure 1 actually extends to $\Delta t = 0$ and would emerge more clearly given more data, ultimately putting PSR J1341–6220 in the Poisson class; or (ii) the correspondence between power-law size and exponential waiting time statistics is not one-to-one (Melatos et al. 2008).

Second, it is apparent by eye that in the two cases where $\hat{p}(s)$ decreases monotonically (PSR J0534+2200 and PSR J1740–3015), $\hat{p}(s)$ is broadly consistent with a power law. The dashed line is consistent with the solid curve and is bracketed by the dotted fits from Melatos et al. (2008), even after adding three events since 2008. Interestingly, the Poisson-like duo have $1.11 \leq a \leq 1.22$ for the best-fitting dashed line, whereas PSR J1341–6220 has $a = 0.92$ ¹⁰. This division is significant physically, because the mean is dominated by different extremes of the distribution in the two cases, with $\langle \Delta \nu \rangle = (a - 1)(2 - a)^{-1}(\Delta \nu_{\max}/\Delta \nu_{\min})^{1-a}\Delta \nu_{\max}$ for $1 < a < 2$ and $\langle \Delta \nu \rangle = (a - 1)(2 - a)^{-1}\Delta \nu_{\max}$ for $a < 1$ (assuming $\Delta \nu_{\min} \ll \Delta \nu_{\max}$).

It is sometimes claimed in the literature that the quasiperiodic glitchers harbor two distinct event populations (Melatos et al. 2008). We find no compelling evidence to support this claim in Figure 4. With $h = h_0$, there are weak hints of two peaks at $s \approx -7.7$ and $s \approx -6.5$ in PSR J0537–6910, the larger events being more frequent. The hypothetical populations are well separated relative to h , but the lesser group contains just four out of 40 events, which are probably random outliers; the validation experiments in Figure 1 routinely produce a few outliers in any given realization, which show up as a small, low- s bump for $N \leq 25$. Likewise, in PSR J1341–6220, the broad plateau in $\hat{p}(s)$ contains a hint of two bumps at $s \approx -7.4$ and $s \approx -6.1$, but again similar noise artifacts are seen in Figure 1. As in Figure 3, using $h = h_0/2$ produces multiple spurious peaks in every object, suggesting this bandwidth is undersmoothing significantly, while $h = 2h_0$ produces a similarly-shaped estimate with a single peak that is broadly consistent with the result for $h = h_0$. More data may alter this picture, but for now the nonparametric case for bimodality in glitch sizes is

⁹ The drop in the PDF at $s < s_{\min}$ is an artifact; it traces the leftward Gaussian tail of the leftmost kernel.

¹⁰Recall from footnote 4 that the PDF of the logarithm of a power law-distributed variable with power law index a is a power law with index $1 - a$, and hence has a positive slope for $a < 1$.

weak in the five objects analysed here.

4. Conclusion

As the number of detected radio pulsar glitches grows, it is ever more feasible to disaggregate the data and construct size and waiting time distributions for individual objects. Previous statistical analyses have assumed theoretically inspired parametric PDFs (e.g. power law, exponential, finite mixture) and tested for K-S inconsistency (Melatos et al. 2008; Espinoza et al. 2011; Konar & Arjunwadkar 2014; Onuchukwu & Chukwude 2016). In this paper, we estimate the PDFs nonparametrically using the kernel density estimator, a powerful tool which converges optimally in many circumstances and has proved its mettle in many applications, where data sets are modest in size (Wand & Jones 1995).

Our analysis yields three main results. (i) It confirms the existence of two classes of glitcher: Poisson-like objects with monotonically decreasing waiting time and size PDFs, consistent with exponential and power-law functional forms respectively, and objects with peaked waiting time and size PDFs, which trigger quasiperiodically. (ii) It suggests that one object which was previously classified as Poisson-like, PSR J1341–6220, shows evidence of hybrid behaviour: $\hat{p}(\Delta t)$ peaks at $\Delta t > 0$, but the peaks in $\hat{p}(\Delta t)$ and $\hat{p}(s)$ are broader than for PSR J0537–6910 and PSR J0835–4510, and $\hat{p}(\Delta t)$ as a whole remains marginally consistent with an exponential distribution in a K-S sense. (iii) One sees weak hints of bimodality in $\hat{p}(\Delta t)$ and $\hat{p}(s)$, consistent with previous parametric modeling of quasiperiodic glitchers (Melatos et al. 2008) and a modest excess of large glitches in aggregate statistics (Lyne et al. 2000). However, Monte-Carlo experiments (Figure 1) and a sensitivity study addressing bandwidth selection in §3.1 and §3.2 present an inconclusive picture. The putative bimodality is as likely to be a noise artifact as not, given the data at hand.

Do the above results shed new light on glitch physics? This complicated question will be addressed in depth in a forthcoming theoretical paper. Here we venture to make one, model-independent point without favoring any of the microphysical mechanisms referenced in §1. It is thought that glitches are driven by the electromagnetic torque, which spins down the stellar crust differentially with respect to internal components. Stresses of various kinds (e.g. elastic forces in the context of crust quakes, Magnus forces in the context of superfluid vortex dynamics) build up globally yet inhomogeneously, until a glitch is triggered, whereupon they relax locally via chains (‘avalanches’) of threshold-activated, stick-slip events (e.g. crust cracking, or vortex unpinning). The avalanches must be cooperative phenomena mediated by a knock-on process, otherwise the central limit theorem predicts size and waiting time PDFs dramatically narrower than those observed, given the large number of interacting

elements involved (e.g. $\gtrsim 10^{10}$ vortices) (Warszawski et al. 2012; Warszawski & Melatos 2013; Fulgenzi et al. 2016). Avalanche systems of this sort, like sand piles, tend towards a self-organized critical state and operate in two regimes: (i) slow driving, where successive events are triggered in spatially distinct regions and are mutually independent, i.e. Poisson-like, with scale-invariant size distributions, and (ii) fast driving, where successive events involve the whole system (e.g. all the vortices in a superfluid, or all the grains in a sand pile) and recur quasiperiodically with roughly equal sizes (Jensen 1998; Melatos et al. 2008). In this sense, therefore, the nonparametric PDF estimates in Figures 3–4 are broadly consistent with theoretical expectations, irrespective of the microphysics. However, three additional implications flow from the new results in this paper. First, with the hybrid behaviour of PSR J1341–6220 defying easy categorization, it makes sense to look harder for independent ways to classify radio pulsars as slowly/rapidly driven in the sense above¹¹. Second, among the quasiperiodic candidates, $\hat{p}(s)$ is considerably narrower in PSR J0835–4510 (≈ 0.5 dex) than in the others (≈ 2.5 dex), and $\hat{p}(\Delta t)$ is relatively broad in PSR J1341–6220 (indeed almost exponential), raising the interesting possibility that the nexus between power-law size and exponential waiting time statistics, characteristic of self-organized criticality, may sometimes be broken. Third, if multimodality is uncovered in any object in the future, as more data are collected, it will argue for the existence of an additional, non-scale-invariant trigger in the glitch mechanism, at least in some pulsars. How this relates (if at all) to the violation of scale-invariance implied by the minimum glitch size resolved in PSR J0534+2200 (Espinoza et al. 2014) is an interesting question for future work.

Acknowledgements

The authors record their warm and respectful gratitude to the late Professor Peter Gavin Hall at the University of Melbourne for his input during the early part of this work, including his recommendation to use the KDE technique and his expert guidance concerning smoothing and edge correction issues. This research was supported by the Australian Research Council through a discovery project grant and the Centre of Excellence for Gravitational Wave Discovery (OzGrav; project number CE170100004).

¹¹ Preliminary analysis of the next most active glitchers, PSR J0631+1036 ($N = 15$) and PSR J1801–2304 ($N = 13$), suggests that the former is Poisson-like, and the latter is quasiperiodic with a broad $\hat{p}(\Delta t)$ like PSR J1341–6220. However, N is too small to interpret the results reliably. More data are needed and will be forthcoming soon, as both objects are active, with $\langle \Delta t \rangle = 1.1$ yr and 2.3 yr respectively.

REFERENCES

- Antonopoulou D., Espinoza C. M., Kuiper L., Andersson N., 2018, *MNRAS*, 473, 1644
- Ashton G., Prix R., Jones D. I., 2017, *ArXiv e-prints*
- Caleb M., Flynn C., Bailes M., Barr E. D., Bateman T., Bhandari S., Campbell-Wilson D., Green A. J., Hunstead R. W., Jameson A., Jankowski F., Keane E. F., Ravi V., van Straten W., Krishnan V. V., 2016, *MNRAS*, 458, 718
- Chaudhuri P., Marron J. S., 1999, *Journal of the American Statistical Association*, 94, 807
- Davis K. B., 1975, *The Annals of Statistics*, pp 1025–1030
- Davis K. B., 1977, *The Annals of Statistics*, pp 530–535
- Espinoza C. M., Antonopoulou D., Stappers B. W., Watts A., Lyne A. G., 2014, *MNRAS*, 440, 2755
- Espinoza C. M., Lyne A. G., Stappers B. W., Kramer M., 2011, *MNRAS*, 414, 1679
- Eya I. O., Urama J. O., Chukwude A. E., 2017, *ApJ*, 840, 56
- Ferdman R. D., Archibald R. F., Gourgouliatos K. N., Kaspi V. M., 2017, *ArXiv e-prints*
- Fuentes J. R., Espinoza C. M., Reisenegger A., Stappers B. W., Shaw B., Lyne A. G., 2017, *ArXiv e-prints*
- Fulgenzi W., Melatos A., Hughes B. D., 2016, *MNRAS submitted*
- Hall P., 1992, *The bootstrap and Edgeworth expansion*. Springer Science & Business Media
- Hall P., Marron J., Park B. U., 1992, *Probability theory and related fields*, 92, 1
- Haskell B., Melatos A., 2015, *International Journal of Modern Physics D*, 24, 1530008
- Janssen G. H., Stappers B. W., 2006, *A&A*, 457, 611
- Jensen H. J., 1998, *Self-Organized Criticality*. Cambridge: University Press
- Konar S., Arjunwadkar M., 2014, *ArXiv e-prints*
- Kramer M., Stappers B., 2010, in *ISKAF2010 Science Meeting LOFAR, LEAP and beyond: Using next generation telescopes for pulsar astrophysics*

- Lyne A. G., Jordan C. A., Graham-Smith F., Espinoza C. M., Stappers B. W., Weltevrede P., 2015, *MNRAS*, 446, 857
- Lyne A. G., Pritchard R. S., Graham-Smith F., 1993, *MNRAS*, 265, 1003
- Lyne A. G., Shemar S. L., Smith F. G., 2000, *MNRAS*, 315, 534
- Marron J., Chung S., 2001, *Computational Statistics*, 16, 195
- Marron J., Nolan D., 1988, *Stat. Probab. Lett.*, 7, 195
- Melatos A., Peralta C., Wyithe J. S. B., 2008, *ApJ*, 672, 1103
- Middleditch J., Marshall F. E., Wang Q. D., Gotthelf E. V., Zhang W., 2006, *ApJ*, 652, 1531
- Monaghan J. J., 2005, *Reports on Progress in Physics*, 68, 1703
- Morley P. D., García-Pelayo R., 1993, *Europhysics Letters*, 23, 185
- Nelson J., Hills R., Cudaback D., Wampler J., 1970, *ApJ*, 161, L235
- Onuchukwu C. C., Chukwude A. E., 2016, *Ap&SS*, 361, 300
- R Core Team 2014, *R: A Language and Environment for Statistical Computing*. R Foundation for Statistical Computing, Vienna, Austria
- Radhakrishnan V., Manchester R. N., 1969, *Nature*, 222, 228
- Reichley P. E., Downs G. S., 1969, *Nature*, 222, 229
- Scott D. W., 1992, *Multivariate Density Estimation*
- Shaw B., Lyne A. G., Stappers B. W., Weltevrede P., Bassa C. G., Lien A. Y., Mickaliger M. B., Breton R. P., Jordan C. A., Keith M. J., Krimm H. A., 2018, *MNRAS*
- Sheather S. J., Jones M. C., 1991, *J. R. Stat. Soc. Ser. B*, 53, 683
- Shemar S. L., Lyne A. G., 1996, *MNRAS*, 282, 677
- Silverman B. W., 1986, *Density estimation for statistics and data analysis*. London: Chapman and Hall
- Wand M., 2014, *KernSmooth: Functions for kernel smoothing for Wand & Jones (1995)*
- Wand M. P., Jones M. C., 1995, *Kernel smoothing*. London: Chapman and Hall

Warszawski L., Melatos A., 2011, MNRAS, 415, 1611

Warszawski L., Melatos A., 2013, MNRAS, 428, 1911

Warszawski L., Melatos A., Berloff N. G., 2012, Phys. Rev. B, 85, 104503

Wong T., Backer D. C., Lyne A. G., 2001, ApJ, 548, 447

Yu M., Liu Q., 2017, ArXiv e-prints

Yu M., Manchester R. N., Hobbs G., Johnston S., Kaspi V. M., Keith M., Lyne A. G., Qiao G. J., Ravi V., Sarkissian J. M., Shannon R., Xu R. X., 2013, MNRAS, 429, 688